JOURNAL OF THE PHYSICAL SOCIETY OF JAPAN, Vol. 37, No. 2, AUGUST, 1974

Infrared Luminescence of Fe^{3+} in $CuGaS_2$ and $CuAlS_2$

Katsuaki SATO and Teruo TERANISHI

Broadcasting Science Research Laboratories of Nippon Hoso Kyokai, Setagaya-ku, Tokyo 157

(Received March 15, 1974)

A sharp luminescence line due to the crystal-field transition ($^4T_1 - {}^6A_1$) of Fe^{3+} in the tetrahedral symmetry is observed for the first time in iron-doped I-III-VI_2 chalcopyrite type compounds, $CuGaS_2$ and $CuAlS_2$. The peak energy is 4,942 cm^{-1} and 5,804 cm^{-1} respectively. These values are rather small as compared to those in many ferric oxides in which the excitation energy of $^4T_1$ in octahedral symmetry is observed around 10,000 cm^{-1}.

The Zeeman effect is also observed and is explained quantitatively by the use of the ligand field theory: We find that $g_\perp$ of the lowest excited state is zero and the spin-orbit parameter 18 cm^{-1}.

§ 1. Introduction

The authors have been working on the optical properties of Fe-ion in the I-III-VI_2 chalcopyrite type semiconductors, $CuGaS_2$ and $CuAlS_2$, in order to obtain some insight to the electronic structures of Fe in the antiferromagnetic semiconductor $CuFeS_2$.

It has been clarified so far that the Fe-ion induces a very strong absorption band in the visible and near-infrared region with peaks at about 10,000 cm^{-1} and 15,000 cm^{-1}.[1,2] In addition, a molecular orbital calculation has suggested that the absorption is caused by the charge-transfer transition from 3p-orbitals of sulphur ligands to the vacant 3d-orbitals of the central Fe^{3+}-ion.[3]

The main purpose of the present paper is to determine the ionic valence of Fe in this type of crystals by observing the crystal-field spectrum of the ion.

A recent report on the ESR analysis of $CuGaS_2$:Fe shows that the Fe-ion becomes trivalent in this crystal.[4] If this is the case, observation of the crystal-field transition of $Fe^{3+}(3d^5)$ by absorption measurements should be very difficult because the transition is spin-forbidden. We, therefore, carried out the luminescence measurements, by which we have found sharp luminescence line spectrum in the near-infrared region.

The Zeeman effect of the luminescence line was also observed. Theoretical analysis of the experiment shows that the luminescence is caused by the crystal-field transition $^4T_1$-$^6A_1$ of Fe^{3+}-ion.

The rest of this article consists of three sections; in § 2 are described the methods and the results of the experiments, in § 3 the theoretical considerations on the results and in § 4 some discussions on unexplained properties of the luminescence.

§ 2. Experiments

2.1 *Experimental techniques*

The single crystals of $CuGaS_2$ and $CuAlS_2$ were grown by the chemical transport in the evacuated silica tube by using iodine as a transport agent. The starting materials were elements of Cu(4*N*), Ga(4*N*) or Al(4*N*) and *S*(4*N*). The crystals were doped with Fe by adding appropriate amounts of FeS powder to the starting materials. Details of the crystal growth are found in the ref. 2.

The obtained crystals were black-faced column like ones or thin platelets. The natural surface was a (112) plane, which for the chalcopyrite structure (D_{2d}) is equivalent to a (111) plane in zinc blende. The orientation of [001] axis is determined by a combination of X-ray studies and observation of the dichroism of the absorption edge.

The optical studies were carried out in a glass dewer by immersing the samples in liquid helium or liquid nitrogen.

In the luminescence measurements without magnetic field, the light path of the excitation was taken to be perpendicular to that of the detection of the luminescence, whereas both paths were arranged collinear in the Zeeman effect measurement in which the magnetic field was perpendicular to the light path. In the

latter case much care was taken to prevent the direct entrance of the excitation beam into the monochromator slit.

The excitation source was a 100 W super high pressure mercury lamp with suitable filters to cut off the light with wavelength of the luminescence. The emitted light was dispersed by the Spex-1800 Czerny-Turner spectrometer mounted with a 600 G/mm grating (the blaze wavelength=1.6 μm) used in the first order. The order selection was done by suitable combination of glass filters.

Light was chopped at 187.5 Hz by a rotating sector and detected by a cooled PbS detector and the signal was amplified by a Lock-in amplifier (PAR model 124) equipped with a paper tape output system for computer-aided data treatments.

The weak emission intensity requires a sufficient width of entrance slit of the spectrometer, which limits the maximum resolution to 0.6 cm^{-1}. The polarization measurements were not carried out throughout this investigation.

In the absorption measurements all equipments were the same as those for the luminescence measurements except the light source, which was a 100 W halogen-tungsten lamp.

For the excitation spectrum measurements a high intensity monochromator with short focal length combined with a 300 W halogen-tungsten lamp was employed as the excitation light source.

2.2 *The optical properties without magnetic field*

The luminescence spectrum of $CuGaS_2$:Fe and $CuAlS_2$:Fe at 4.2 K consists of a main line and a train of side lines in its low energy side.

The 4.2 K spectra in the vicinity of the main line are illustrated in the Fig. 1(a) and (b). The main line of $CuGaS_2$:Fe is a doublet in which the separation between the two peaks is 1.3 cm^{-1} and the intensity ratio is about 10:1. On the other hand the spectrum of $CuAlS_2$:Fe consists of several broader components.

The peak position and the line width of each spectrum are given in Table I together with some additional informations of the compounds.

At higher temperatures the lineshapes become broader and the peaks become smaller. The 77 K spectra are given in Fig. 2(a) and (b). Note that the energy scale of Fig. 2 is much

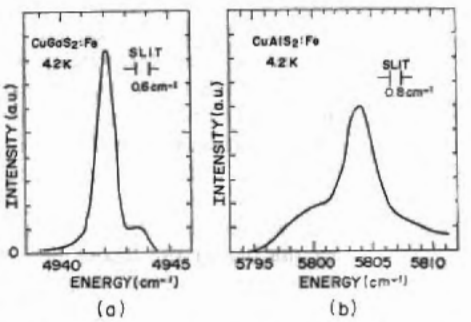

Fig. 1. The luminescence spectra of (a) $CuGaS_2$:Fe and (b) $CuAlS_2$:Fe at 4.2 K.

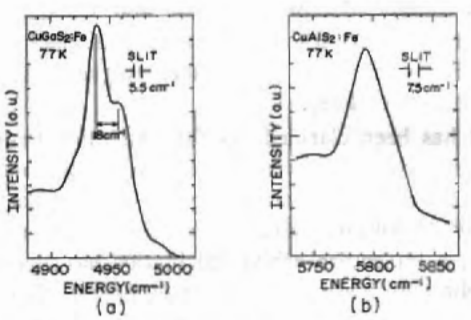

Fig. 2. The luminescence spectra of (a) $CuGaS_2$:Fe and (b) $CuAlS_2$:Fe at 77 K. Note that the energy scale of this figure is much different from that of Fig. 1.

different from that of Fig. 1. Figure 2(a) shows a 'hot' line at 18 cm^{-1} higher photon energy than the main line. The line suggests the existence of a higher state separated by 18 cm^{-1} from the lowest excited state.

At the energy position where the main luminescence line is observed (4,942 cm^{-1}), is observed a very weak absorption line in $CuGaS_2$:$Fe_{0.008}$. It confirms that the main line is the

Table I. The position ν(cm^{-1}) and $\Delta\nu$(cm^{-1}) of the zero line. The lattice constants a_0(Å), c_0(Å), the energy band gap Eg(cm^{-1}) and the peak positions of the charge-transfer absorption band E_A(cm^{-1}), E_B(cm^{-1}) are also listed.

Substance	ν	$\Delta\nu$	a_0	c_0	Eg	E_A	E_B
$CuGaS_2$:$Fe_{0.008}$	4942.3±0.2	1.0	5.3499	10.479	20,400	9,600	15,000
$CuAlS_2$:$Fe_{0.008}$	5804.0±0.5	3.0	5.3286	10.430	27,000	10,400	16,000

Table II. The energy separations between the zero line and the side lines. Previously reported data on the phonon energies for $CuGaS_2$, $CuAlS_2$ and ZnS are also given.*

$CuGaS_2$:Fe	Present study	77,	99,	117,	157,	162,	174,	279,	308,	332,	355,	365, 379
	Bhar *et al.*[14]									328, (*LO*)	358, (*TO*)	365 (*LO*)
$CuAlS_2$:Fe	Present study	74,	94,	119,	136,	144,	180,	221,	279,	319,		441, 464
	Bhar *et al.*[14]										398, (*TO*)	439, 462 (*TO*) (*LO*)
ZnS	Slack *et al.*[6]			115, (*TA*)					300, (*TO*)		350 (*LO*)	

zero-phonon line of the transition. The absorption coefficient of the peak is 8 cm^{-1} and the line width is 8 cm^{-1}, from which the oscillator strength of the transition is estimated to be 2.2×10^{-7} using the nominal value of iron concentration.

In Fig. 3(a) and (b) the spectra of the side lines are illustrated. These lines are considered to be the vibronics attached to the zero line. The peak positions of the side lines measured from the zero-line is listed in Table II together with the infrared absorption data of the phonon energy.

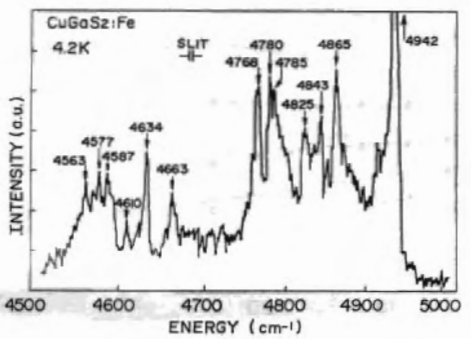

(a)

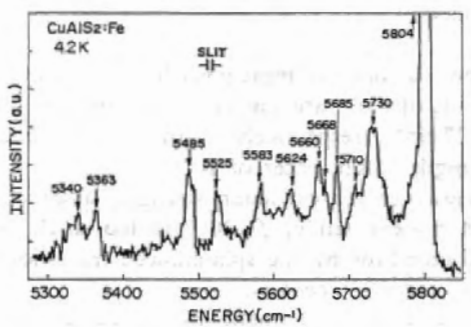

(b)

Fig. 3. The side lines in the luminescence spectra of (a) $CuGaS_2$:Fe and (b) $CuAlS_2$:Fe. The peak intensity of each side line is not more than 1/10 of that of the zero line.

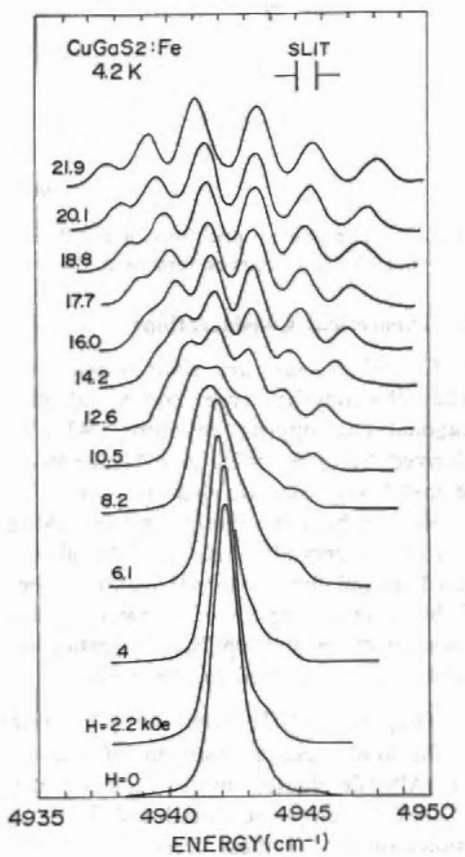

Fig. 4. The Zeeman spectra of the zero line of $CuGaS_2$:Fe at 4.2 K. The spectra are arbitrarily shifted for the sake of clarity.

* *Note added in proof*—W. H. Koschel *et al.* recently reported a detailed analysis of the optical phonon spectrum of $CuAlS_2$ by infrared reflectivity and Raman scattering measurements. Their data allows us to interpret most of the side-lines listed in Table II in terms of the phonon side bands. (Solid State Commun. 13 (1973) 1011.)

In the next place the excitation spectrum of the i.r. emission of $CuGaS_2:Fe_{0.001}$ is studied. It is found from this measurement that the luminescence is excited by the broad band with photon energies between 7,000 cm^{-1} to 20,000 cm^{-1}. It should be noted that in the same energy region lies the strong absorption band due to the charge-transfer transition relating to Fe^{3+}-ion.

3.3 Zeeman effect

Zeeman effect of the zero-phonon emission line of $CuGaS_2:Fe_{0.0001}$ was measured with a magnetic field up to 22 kOe applied in a (112) plane along the [110] direction of the crystal.

In Fig. 4 are illustrated the Zeeman spectra for various magnitudes of the magnetic field. The peak energies are plotted by circles against the magnetic field in Fig. 5. The peaks represented by black circles have more intensities than those by open circles. At 22 kOe the spectrum consists of six well-defined peaks with intensity ratio of 6:15:25:23:12:6 (arranged in order of increasing energy). The intensity ratio is fairly symmetric and it indicates that the Zeeman effect is due to the splitting of the ground state of the transition.

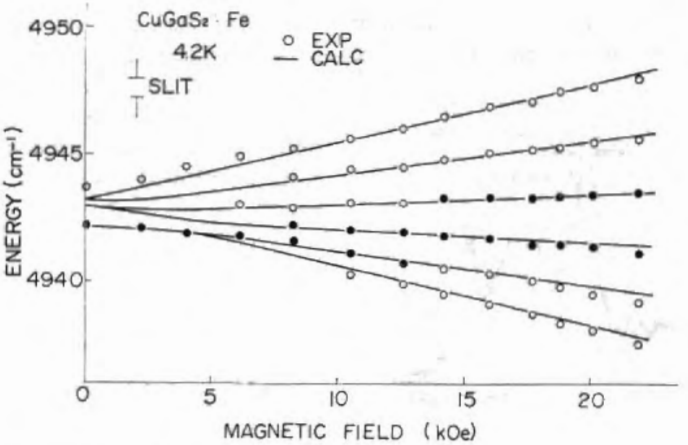

Fig. 5. The energy positions of the Zeeman split peaks. Circles denote the experimental values and the solid curves represent the calculated values.

§3. Theoretical Considerations

3.1 Crystal structure and point symmetry

The chalcopyrite type compound has the tetragonal chalcopyrite structure, $I\bar{4}2d$, which is derived from the cubic zinc blende structure. The metal ion is surrounded by a tetrahedron of anions, which is slightly distorted along the *c*-axis of the crystal. The anion tetrahedra are twisted around the tetragonal *c*-axis of the unit cell by a small angle $\pm\tau$. However it has no serious effect on the optical properties of the crystal and is neglected in the paper.

3.2 Assignment of the transition of the emission

Is the luminescence spectrum of $CuGaS_2:Fe$ or $CuAlS_2:Fe$ caused by Fe^{2+}, Cu^{2+} or Fe^{3+}? Fe^{2+} or Cu^{2+} might be introduced by a break of stoichiometry in these crystals.

The crystal-field spectra of Fe^{2+} and Cu^{2+} in ZnS, a binary analogue of $CuGaS_2$, have been studied by several authors and it has been reported that the transitions ^5E-$^5T_2$ of Fe^{2+} and $^2T_2$-^2E of Cu^{2+} are observed at 2,900 cm^{-1} and 6,927 cm^{-1} respectively with the oscillator strength of the order of 10^{-4}.[5-8]

However the oscillator strength observed in our present study, $f\sim10^{-7}$ is too small to be accounted for by the spin-allowed transitions of Fe^{2+} and Cu^{2+} centers.

The ESR experiment by Schneider *et al.* clearly shows that the Fe-ion becomes trivalent in this compound. Our Zeeman effect measurement also suggests that the ground state is a sextet state, accordingly we assume the presence of a $Fe^{3+}(^6A_1)$ center.

The energy level diagram for $Fe^{3+}(3d^5)$ in the tetrahedral symmetry is shown in Fig. 6,[9] from which we know that the ground state is $^6A_1$ and the lowest excited state is $^4T_1(t_2^3e^2)$ or $^2T_2(t_2e^4)$.

The observed oscillator strength, 10^{-7} is rather too large for a strongly forbidden transition,

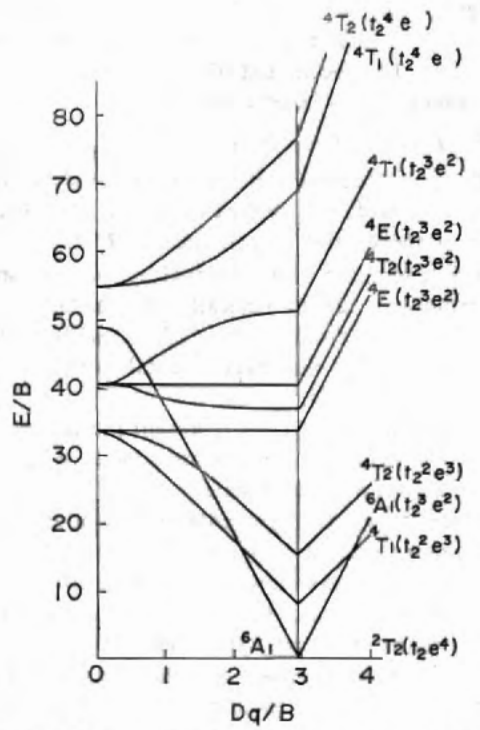

Fig. 6. An energy level diagram of $Fe^{3+}(3d^5)$ in the tetrahedral symmetry.

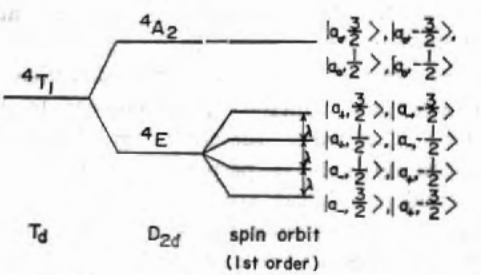

Fig. 7. A proposed energy level scheme for the excited state ($^4T_1$) of Fe^{3+} with a tetragonal distortion (D_{2d}) and a spin-orbit interaction. In this figure $a_\pm=\mp1/\sqrt{2}(\alpha\pm i\beta)$ and $a_0=\gamma$.

$^2T_2-{}^6A_1$ but quite reasonable for $^4T_1$-$^6A_1$ in the tetrahedral symmetry.

$^4T_1$ (with basis functions α, β and γ) in the T_d symmetry splits into $^4A_2(\gamma)$ and $^4E(\alpha,\beta)$ due to the lower symmetry D_{2d}. We assume *a priori* that the splitting is large enough to treat a spin-orbit interaction as a perturbation to $^4A_2$ and ^4E. The interaction does not split $^4A_2$ in the first order. On the other hand ^4E is split into four Kramers doublets equally spaced with energy separation λ, which is expressed by one electron spin-orbit parameter ζ as $\lambda=\zeta/6$. ($\zeta\sim+400\,cm^{-1}$) We also assume that ^4E is lower in energy than $^4A_2$ due to the compressive nature of the tetragonal distortion.

Under these assumptions the excited states are described by wave functions $|\Gamma\gamma',\ M_s'>=|^4E\,a_\pm,\ \pm3/2,>$, $|^4E\,a_\pm,\ \pm1/2>$, $|^4A_2\,a_0,\ \pm3/2>$, and $|^4A_2\ a_0,\ \pm1/2>$ where $a_\pm=\mp1/\sqrt{2}(\alpha\pm i\beta)$ and $a_0=\gamma$, as visualized in the energy diagram of Fig. 7; the lowest excited state is represented by $|^4E\,a_-,\ 3/2>$ and $|^4E\,a_+,\ -3/2>$.

3.3 *Spin Hamiltonian for a Fe^{3+}-ion in D_{2d}*

The spin Hamiltonian appropriate to an Fe^{3+}-ion in D_{2d} symmetry is

$$\mathcal{H}=g\beta\boldsymbol{H}\cdot\boldsymbol{S}+D(S_z^2-35/12)+(7/36)F\{S_z^4-(95/14)S_z^2+81/16\}+(a/6)(S_x^4+S_y^4+S_z^4-707/16). \quad (1)$$

This formula is essentially the same as given in the ref. 4 but we neglect the small displacement of anion ligands from ideal positions in this formulation.

Denoting the angle between H and the z-axis as θ, and the angle between the xy-plain projection of H and the x-axis as ϕ, the eq. (1) is rewritten as follows:-

$$\mathcal{H}=g\beta HS_z\cos\theta+D(S_z^2-35/12)+(7/24)\times\{a+(2/3)F\}\{S_z^4-(95/14)S_z^2+81/16\}+(1/2)g\beta H(e^{-i\phi}S_+ +e^{i\phi}S_-)\sin\theta+(a/48)(S_+^4+S_-^4)\,. \quad (2)$$

The parameters of this Hamiltonian are given by ESR analysis[4] as

$$g=2.024,\ D=0.1885\,cm^{-1},\ a+(2/3)F=0.0103\,cm^{-1},\ a=0.0069\,cm^{-1}\,. \quad (3)$$

We also assume that g is isotropic i.e. $g_{/\!/}=g_\perp$ in the eq. (2).

3.4 *Analysis of the luminescence spectrum in the absence of magnetic field*

The electric dipole transition between the ground state $^6A_1(t_2^3e^2)$ and the excited state $^4T_1(t_2^2(^3T_1)e^3)$ of Fe^{3+} becomes allowed by the perturbation of the spin-orbit interaction. For the sake of simplicity we take only the lowest $^4T_1$ state for the intermediate state. Then the electric-dipole transition matrix $\mathcal{M}^{(\alpha)}_{M_s,M_s'\Gamma'}$ is given by

$$\mathcal{M}^{(\alpha)}_{M_s,M_s'\Gamma'}=\sum_{Ms''\Gamma''}\frac{\langle t_2^3e^2\,{}^6A_1M_s|V\mathrm{so}|t_2^3(^3T_1)e^3\,{}^4T_1\gamma''Ms''\rangle}{W(^6A_1)-W(^4T_1)}\times\langle t_2^2(^3T_1)e^3\,{}^4T_1\gamma''Ms''|P^{(\alpha)}|t_2^2(^3T_1)e^3\,{}^4T_1\gamma'Ms'\rangle\,, \quad (4)$$

where Vso denotes the spin-orbit operator, $W(^6A_1)$ and $W(^4T_1)$ the averaged energies for $^6A_1$ and $^4T_1$ respectively, $P^{(\alpha)}$ the electric dipole

operator for the light with $E//\alpha(\alpha=x,\ y$ or $z)$, and the final state $|\gamma', Ms'>$ takes any one of the excited states illustrated in Fig. 7. The matrix element (4) can be estimated by using the similar procedures as employed in the interpretation of the absorption spectrum of Al_2O_3: Cr^{3+}.[10] The transition intensity calculated for the unpolarized light

$$|\mathscr{M}|^2=1/3\{|\mathscr{M}^{(x)}|^2+|\mathscr{M}^{(y)}|^2+|\mathscr{M}^{(z)}|^2\},$$

is given in Table III.

In the table p denotes

$$p=\frac{\langle T_1||P(T_2)||T_1\rangle\cdot\zeta'}{\sqrt{6}(W(^6A_1)-W(^6E))},$$

where the double-barred matrix element means the reduced matrix element of the electric dipole and ζ' denotes a non-diagonal matrix element of the spin-orbit interaction for one electron.

The eigenvalues of the ground state spin Hamiltonian (2) for zero magnetic field are

$$\left.\begin{aligned} W_{\pm5/2}&=0.6335\ \mathrm{cm}^{-1},\\ W_{\pm3/2}&=-0.1412\ \mathrm{cm}^{-1},\\ W_{\pm1/2}&=-0.4924\ \mathrm{cm}^{-1}. \end{aligned}\right\} \quad (5)$$

We can, therefore, predict a zero-field spectrum for a transition from the lowest excited state denoted by $|a_-, +3/2>$ and $|a_+, -3/2>$ to the ground state multiplets as in Fig. 8, by using the eigenvalues given in eq. (5) and the transition intensity listed in Table III; the predicted values of the zero-field splitting 1.12 cm^{-1} and the intensity ratio 10:3 are very close to the observed ones of 1.3 cm^{-1} and 10:1.

The hot line observed in Fig. 2(a) corresponds to another spin-orbit split level $|a_-, 1/2>$ or $|a_+, -1/2>$, with spin-orbit parameter $\lambda=18\ cm^{-1}$. This rather small value of the spin-orbit splitting should be compared with the case of MnF_2 in which the spin-orbit splitting of the zero-magnon line of $^4T_1$ is 17 cm^{-1}.[11] It should be pointed out that the reduction of the spin-orbit coupling has been explained in terms of a dynamical Jahn-Teller effect.[12,13]

3.5 *Analysis of the Zeeman effect*

In our Zeeman effect measurements the magnetic field was applied along the [110] direction of the crystal, which means $H\perp z$.

We computed the eigenvalues of the spin Hamiltonian (2) numerically for each of 23 values of H from 0 to 22 kOe with 1 kOe interval, under the experimental condition of $\theta=\pi/2$ and $\phi=\pi/4$.

Solid curves in Fig. 5 represent the calculated energy positions under the assumption of $g_\perp=0$ for the lowest excited state.

Since previous arguments have shown that the lowest excited state is represented by $Ms=\pm3/2$ and the next lowest state with $Ms=\pm1/2$ is $+18\ cm^{-1}$ apart, the $\pm3/2$ state does not split when the magnetic field of 20 kOe is applied perpendicular to the z-axis. This supports the above assumption that $g_\perp$ is zero. The same argument is valid for any other split components of ^4E i.e. $g_\perp(^4E)=0$.

In the next place we calculate the intensity ratio of the Zeeman spectrum. In the high field limit it is convenient to quantize the spin of the ground state along the direction of magnetic field which is perpendicular to the z-axis. The wave functions, in which the quantization axis is perpendicular to z, are expressed as a linear combination of those in which the quantization axis is z. The transition intensities for the new wave functions are calculated by using the eq. (4) and are listed in Table IV; the calculated intensity ratio for the luminescent transition from the lowest excited state agrees very well with the observed one.

Table III. The intensities of transitions between the ground state $^6A_1\,|Ms>$ and the excited state $^4T_1\,|^4\Gamma\gamma', Ms'>$ ($^4\Gamma\gamma'=^4E\,a_\pm$ or $^4A_2\,a_0$) in the absence of magnetic field.

$^4\Gamma$ / $\lvert\gamma', Ms'\rangle$	^4E				$^4A_2$	
	$\lvert a_+, 3/2\rangle$	$\lvert a_+,1/2\rangle$	$\lvert a_+,-1/2\rangle$	$\lvert a_+,-3/2\rangle$	$\lvert a_0,3/2\rangle$	$\lvert a_0,1/2\rangle$
$^6A_1\,\lvert Ms\rangle$	$\lvert a_-,-3/2\rangle$	$\lvert a_-,-1/2\rangle$	$\lvert a_-,1/2\rangle$	$\lvert a_-,3/2\rangle$	$\lvert a_0,-3/2\rangle$	$\lvert a_0,-1/2\rangle$
$\lvert\pm5/2\rangle$	30			10		
$\lvert\pm3/2\rangle$		18	6		16	
$\lvert\pm1/2\rangle$	1	3	9	3		24

$\times|p|^2/30$

Table IV. The intensities of transitions under the magnetic field which is perpendicular to z.

^4T / $\|\gamma', Ms'\rangle$	^4E				$^4A_2$	
	$\|a_+,3/2\rangle$	$\|a_+,1/2\rangle$	$\|a_+,-1/2\rangle$	$\|a_+,-3/2\rangle$	$\|a_0,3/2\rangle$	$\|a_0,1/2\rangle$
$^6A_1$ $\|Ms\rangle$	$\|a_-,-3/2\rangle$	$\|a_-,-1/2\rangle$	$\|a_-,1/2\rangle$	$\|a_-,3/2\rangle$	$\|a_0,-3/2\rangle$	$\|a_0,-1/2\rangle$
$\|+5/2\rangle$	5	15	15	5	10	30
$\|+3/2\rangle$	19	21	9	7	18	6
$\|+1/2\rangle$	38	6	6	14	4	12
$\|-1/2\rangle$	38	6	6	14	4	12
$\|-3/2\rangle$	19	21	9	7	18	6
$\|-5/2\rangle$	5	15	15	5	10	30

$\times |p_i|^2/120$

For intermediate magnitudes of the magnetic field one can calculate the transition intensity by employing the numerically-computed eigenvectors of the ground state spin Hamiltonian (2); the Zeeman spectra thus predicted are visualized in Fig. 8, which explains quite satisfactorily the observed Zeeman spectra shown in Fig. 4.

§ 4. Conclusion and Discussion

The present studies have clarified firstly that the observed i.r. luminescence is caused by the crystal-field transition $^4T_1$-$^6A_1$ of Fe^{3+}, secondly that the excited state is well described by the states $|a_-, +3/2\rangle$ and $|a_+, -3/2\rangle$ which are the split components of the $^4T_1$ state due to the lower symmetry (D_{2d}) and the spin-orbit

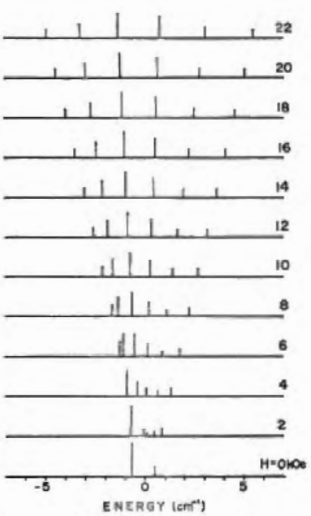

Fig. 8. The predicted Zeeman spectra for various magnitudes of the magnetic field. The excited state is assumed to be represented by $|a_-, +3/2\rangle$ and $|a_+, -3/2\rangle$.

interaction, thirdly that $g_\perp$ for the lowest excited state is zero and lastly that the spin-orbit splitting is rather small probably due to the dynamical Jahn-Teller effect.

The present studies have thus confirmed the presence of the trivalent state of Fe-ion in the I-III-VI_2 chalcopyrite type compounds.

The most important problem left is why the transition energy takes such a small value as 5,000 cm^{-1} in contrast to many ferric oxides in which the transition of $^4T_1$-$^6A_1$ in the octahedral site appears in the vicinity of 10,000 cm^{-1}.

If the smallness of the observed transition energy were to be explained by the reduction of B (Racah's parameter for the Coulomb interaction), its value should be as small as 1/3 of that of free ion. Since such a large reduction of B seems to be unnatural, another mechanism should be sought to explain the anomalous lowering of the $^4T_1$ state.

As stated in § 1 there exists a strong charge-transfer absorption band only several thousand cm^{-1} apart in energy from the crystal-field transition. We also find that the luminescence is excited by the light of the same photon energy region as the strong charge-transfer absorptions.

We, therefore, propose a model in which the mixing of $Fe^{3+}(3d^5)$ states and Fe^{2+}—$S^-(3d^6+3p\text{-hole})$ charge-transfer states due to a configuration interaction plays an important rôle in lowering of the transition energy. A further theoretical research on this model is now progressing.

We also attribute the large g shift ($\Delta g \sim 0.02$) and the large anisotropy ($D \sim 0.2\,cm^{-1}$) to the anomalous lowering of the excited states.

Acknowledgements

The authors are very grateful to Professor S. Sugano for his continuous encouragement and advices to this work. They are also indebted to Dr. K. Aoyagi, Dr. T. Kambara and Dr. S. Washimiya for their helpful discussions.

References

1) K. Kondo, T. Teranishi and K. Sato: J. Phys. Soc. Japan **36** (1974) 311.
2) T. Teranishi, K. Sato and K. Kondo: J. Phys. Soc. Japan **36** (1974) 1618.
3) T. Kambara: J. Phys. Soc. Japan **36** (1974) 1625.
4) J. Schneider, A. Räuber and G. Brandt: J. Phys. Chem. Solids **34** (1973) 443.
5) G.A. Slack, F.S. Ham and R.M. Chrenko: Phys. Rev. **152** (1966) 376.
6) G.A. Slack and B.M. O'Meara: Phys. Rev. **163** (1967) 335.
7) I. Broser, H. Maier and H.J. Schulz: Phys. Rev. **140A** (1965) 2135.
8) I. Broser, U. Scherz and M. Wöhlecke: J. Luminescence **1, 2** (1970) 39.
9) Y. Tanabe and S. Sugano: J. Phys. Soc. Japan **9** (1954) 766.
10) S. Sugano and Y. Tanabe: J. Phys. Soc. Japan **13** (1958) 880.
11) R.L. Greene, D.D. Sell, W.M. Yen and A.L. Schawlaw: Phys. Rev. Letters **15** (1965) 656.
12) F.S. Ham: Phys. Rev. **138A** (1965) 1727.
13) S. Washimiya and K. Gondaira: J. Phys. Soc. Japan **23** (1967) 1.
14) G.C. Bhar and R.C. Smith: Phys. Status solidi (a) **13** (1972) 157.